$K\alpha$ and $K\beta$ x-ray emission spectra of metallic scandium

Dimitrios F. Anagnostopoulos,[1,*] Ruth Sharon,[2] Detlev Gotta,[1] and Moshe Deutsch[2,†]
[1]*Institut für Kernphysik, Forschungszentrum Jülich, D-52425 Jülich, Germany*
[2]*Physics Department, Bar Ilan University, Ramat Gan 52900, Israel*
(Received 19 February 1999)

The $K\alpha$ and $K\beta$ spectra from metallic scandium, the first of the $3d$ transition elements, were measured using a high-resolution curved crystal spectrometer. The spectrometer resolution was determined employing a narrow emission line from pionic neon. The parameters of the resolution-corrected spectrum are extracted and compared to previous studies and theory. Fits to *ab initio* relativistic Dirac-Fock calculated spectra show that the $K\alpha$ spectrum can be accounted for using an isolated-atom model with diagram, $\underline{3d}$- and $\underline{3p}$- spectator hole transitions. The $K\beta$ spectrum, however, cannot be fitted by such isolated-atom multiplets and may require employing nonlocalized bonding orbitals. [S1050-2947(99)04709-5]

PACS number(s): 32.30.Rj, 32.80.Hd, 31.30.Jv

I. INTRODUCTION

High-resolution x-ray fluorescence spectroscopy is one of the most powerful tools for chemical-state analysis of new materials. The structure of satellite lines is highly sensitive to differences in chemical bonding up to the third row in the Periodic Table of elements and this fact is extensively used for chemical-state characterization on solid materials [1]. The x-ray emission spectra of the $3d$ transition metals exhibit several peculiar characteristics, not observed in other elements. The most prominent of these is skewed line shapes, the origin of which is still under investigation and debate [2,3]. Several mechanisms such as shake-off and shake-up [4], conduction-band collective excitations [5], exchange [6], and final-state interactions [7] were suggested to account for this effect. In a recent study we have combined precision line-shape measurements and *ab initio* relativistic Dirac-Fock calculations to show that the skewed line shapes of the Cu $K\alpha$ and $K\beta$ spectra can be fully accounted for by assuming contributions from the diagram and $\underline{3d}$-spectator transitions only [3] (in the following, an underline denotes hole states). Measurements on other transition metals are, however, indispensable for supporting this interpretation and for establishing Z-dependent trends in this behavior for the $3d$ elements. Scandium, having a single $3d$ electron in its nominal $[\mathrm{Ar}]3d^1 4s^2$ ground-state configuration, is the first $3d$ transition metal. This position renders it of special interest in elucidating trends in the relative importance of the $\underline{3d}$-spectator transitions across the group.

Other related issues are the origins of the $K\alpha''$ and $K\beta''$ satellite lines on the high-energy side of the corresponding $K\alpha_1$ and $K\beta_{1,3}$ lines. Scott [8] carried out nonrelativistic Hartree-Fock calculations of the $\underline{3p}$-spectator $\underline{1s3p} \rightarrow \underline{2p3p}$ transition multiplet. Based on the good energy alignment of the strongest line of the calculated multiplet with the measured $K\alpha''$ line positions [9] for atomic numbers $Z=19$–23, he assigned this satellite to the $\underline{3p}$-spectator transition, as originally suggested by Druyvesteyn [4] and supported by the early measurements of Parratt [9]. More recently, Kawai *et al.* [10] studied experimentally the $K\alpha''$ and $K\beta''$ satellites in Sc and its compounds. They conclude that while $K\alpha''$ originates from an *atomic* $\underline{3p}$-spectator $\underline{1s3p} \rightarrow \underline{2p3p}$ transition, the $K\beta''$ satellite most likely results from a $\underline{3p}$-spectator transition of a $3p$ electron coming from the antibonding molecular orbital formed between the $3p$ orbital of the active Sc atom and those of adjacent Sc atoms.

Well-resolved measurements of the scandium $K\alpha_{1,2}$ and $K\beta_{1,3}$ spectra were published only twice, to the best of our knowledge. The first of these, the early study of Parratt [9], concentrated on the $K\alpha''$ satellite of Sc, and employed an insulator, Sc_2O_3, rather than metallic Sc. As shown in the second study, Kawai *et al.* [10], the valence state of the atom has a profound effect on the line shapes and related parameters of the spectrum such as width, position, relative intensity, and asymmetry. However, even the very detailed study of Kawai *et al.* investigated mostly the dependence of the spectra on the chemical state of Sc, by intercomparing the spectra obtained from the metal and several scandium compounds. Although the origins of the spectra of elemental Sc were discussed, no attempt was made in that study to reproduce the line shape theoretically and determine the contributing *atomic* processes. The collective, solid-state contributions to the satellites accompanying the diagram transition were, however, addressed in that study by discrete-variational (DV) $X\alpha$ molecular structure calculations.

The present study focuses on the atomic origins of the spectral line shapes, and tries to identify the contributing transitions based on relativistic Dirac-Fock *ab initio* calculations. It is important to note that our calculations are atomic, rather than molecular or band-structure ones, assuming implicitly an isolated-atom model for the emitting scandium. Agreement of the calculations with the measurements should imply, therefore, that the emission process of these spectra is an atomic and not a collective solid-state process. Unlike previous studies, our measurements were done by the same spectrometer for both the $K\alpha$ and $K\beta$ spectra. More importantly, the resolution of our spectrometer was characterized

*Present address: University of Ioannina, GR-45110 Ioannina, Greece. Electronic address: danagno@nrt.cs.uoi.gr
†Electronic address: deutsch@alon.cc.biu.ac.il

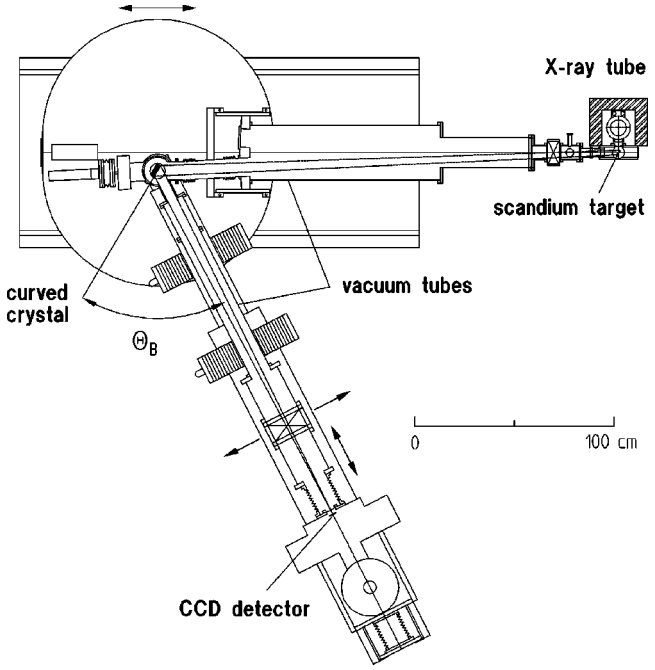

FIG. 1. Setup of the spectrometer with x-ray tube, fluorescence target, Bragg crystal, and CCD x-ray detector.

and determined independently by using extremely narrow emission lines originating in pionic atom transitions [11] at energies close to that of the Sc spectra. The independent determination of the resolution allows a reliable determination of the basic parameters of the emission lines, such as widths, asymmetry indices, etc. We have also carried out detailed fits of the calculated spectra to the measured ones to determine the processes underlying the lineshape, assessing their relative contributions. The fits reveal that the $K\alpha$ spectrum can be accounted for well assuming transitions within a single, isolated atom. A large contribution from $\underline{3d}$-spectator transitions is found, similar to that found for Cu. Our results support an *atomic* $\underline{3p}$-spectator origin for both the $K\alpha''$ and $K\beta''$ satellites. The $\overline{K\beta}$ spectrum, by contrast, cannot be accounted for within the isolated-atom approximation, and probably originates in transitions involving molecular orbitals, supporting the conclusion of Kawai *et al.* [10].

II. EXPERIMENT

A. Setup

For the measurement of the x rays a Johann-type reflection crystal spectrometer was used, which has been designed to investigate x rays in the few-keV range emitted from exotic atoms [11,12]. The spectrometer is shown in Fig. 1 and described in detail elsewhere [13]. The use of focusing Bragg crystals increases considerably the spectrometer's efficiency, and for extended x-ray sources in combination with position-sensitive detectors, placed on the Rowland circle, allows the simultaneous recording of the spectra over finite energy intervals [14]. Intervals of 23 and 33 eV could be recorded simultaneously near the $K\alpha_{1,2}$ and $K\beta_{1,3}$ lines, respectively, without rotating the analyzer.

The scandium atoms were excited by means of either a tungsten- or a chromium-anode sealed x-ray tube installed in front of the 50-μm Mylar window of a chamber containing the Sc fluorescence target. The x-ray beam from the tube was collimated perpendicular to the target-crystal line of sight. The metallic 30 mm$\times$20 mm scandium target, mounted on an aluminum plate, was oriented at 45° to this line.

A spherically bent silicon 220 crystal analyzer was employed in the scandium $K\alpha$ and $K\beta$ measurements. The Sc $K\alpha_1$ and $K\beta_{1,3}$ transition energies of 4090.6 eV and 4460.5 eV, respectively [15], correspond to Bragg angles of 52.12° and 46.37°. The analyzer crystal, 0.3 mm thick, had a circular shape of 95 mm in diameter, and it was glued onto a glass lens, which created a spherical bending to a radius of 2985.4 mm. The crystal and its support were installed on a rotary table connencted to a high-precision angular encoder, allowing us to measure relative rotations with an accuracy of $\pm 0.3''$. To avoid absorption losses, the whole spectrometer, from the Sc target to the charge-coupled device (CCD) detector's window, including the crystal, was kept in vacuum. Metal bellows allowed for changes in the Bragg angle within a range of $\sim 10°$ without breaking vacuum.

The partial focusing perpendicular to the dispersion plane provided by the spherical bending allowed for the use of a CCD as a two-dimensional position-sensitive x-ray detector [16]. The detector was placed in the focal position at the Rowland circle perpendicular to the direction of the Bragg-reflected photons. The total sensitive area of the detector was 17×52 mm^2 (width$\times$height), consisting of a vertical array of two CCD chips separated by a 6-mm gap and having a pixel size of 22.5 μm$\times$22.5 μm. For the presentation of the measured spectra, five CCD pixels were binned together to form a single detector channel, of 112.5 μm total width. Due to the finite vertical extension of target and crystal, the two-dimensional photon distribution in the detector plane was extended over more than the total detector height. The overlap of the reflected radiation cone and the sensitive area of the CCD was about 65%. The reflection image had a parabolic shape, within the height of the detector, originating from the intersection of the crystal-reflected photon cone and the detector's plane. Using the known geometry of the ray trajectories from the source to a given pixel on the detector, the parabolic image on the CCD was transformed to a straight line, perpendicular to the dispersion plane, and subsequently projected onto the dispersion plane, yielding the spectrum vs x, the position along the detector in the dispersion plane [13]. As each of the two spectral ranges was measured without rotating the analyzer, the length scale x on the CCD in the dispersion plane was converted into a relative energy scale E using the linear dispersion dE/dx. The variation of the dispersion with x (i.e., with energy) has been incorporated into our analysis.

The absolute energy scale was fixed by assigning to the peak position of either the $K\alpha_1$ or the $K\beta_{1,3}$ line the literature value [15], which is known to ± 0.4 eV. This is, then, the *absolute* energy scale accuracy of our measurements. The *relative* accuracy is, however, determined by the positional accuracy of the CCD pixels and the accuracy with which the linear dispersion dE/dx is known. dE/dx is determined by the angular dispersion discussed in the next section and is a function of the crystal's radius of curvature, the crystal-detector distance, the energy E, and the crystal characteristics (Bragg-plane repeat distance and the order of reflection). The

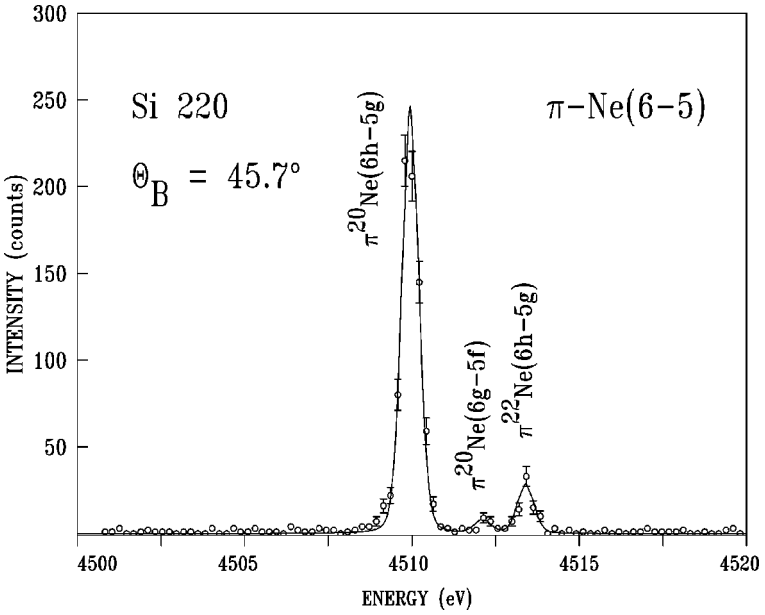

FIG. 2. The π^-Ne$(6\rightarrow5)$ x-ray emission spectrum, as measured with the present spectrometer. A fit with a Gaussian resolution function to the individual emission lines is also shown (line). The $(6h\rightarrow5g)$ line was used to determine the resolution of the spectrometer in this energy range, which is near that of the Sc $K\alpha$ and $K\beta$ spectra.

uncertainty in the linear dispersion is determined by the ±0.5 mm uncertainty in the detector-crystal distance and the ±0.4 eV uncertainty in the absolute energy, and is calculated to be $\pm0.06\%$. With our measurements' statistics the uncertainty in the determination of the position on the CCD was about one-tenth of the pixel size (22.5 μm). This results in few ppm accuracy in the *relative* energy, dE/E, determination. For example, for the Sc $K\alpha_{1,2}$ spectrum, the positional uncertainty of ~3.3 μm translates into a relative energy accuracy of $dE/E\approx1$ ppm. A more detailed analysis is outside the scope of this paper, and is given elsewhere [13].

B. Response function

The response function of the spectrometer was determined from the x-ray emission spectrum of the $(6h\rightarrow5g)$ transition in pionic ^{20}Ne, whose natural width is negligibly small. The measurement was performed in the πE5 area at the Paul-Scherrer-Institute. The energy of the $6h\rightarrow5g$ transition of π^{20}Ne, 4509.89 eV [17], is close to the energies of the Sc lines addressed here. The corresponding Bragg angle is 45.72° and the spectrometer's angular dispersion is $\Delta E/\Delta\theta=21.33$ meV/sec. Two different Si (220) crystals were used in this experiment, denoted ''A'' and ''B.'' The πNe$(6\rightarrow5)$ spectrum, measured using crystal B, is shown in Fig. 2. The line shape of the π^{20}Ne$(6h\rightarrow5g)$ transition is described well by a single Gaussian resolution function with full width at half maximum (FWHM) of $(29\pm2)''$ for crystal A and $(26\pm2)''$ for crystal B.

The rocking curve width of the Si 220 reflection was calculated to be 12.63″ [18]. The natural width of the pionic transition is 12 meV, corresponding to only 0.56″, and thus negligible in comparison with the crystal's rocking curve width and also with the geometrical aberrations originating from the bent crystal setup. The geometrical broadening is dominated by the horizontal extension of the crystal. The aberration originating in the crystal's vertical extension is reduced considerably by the application of the curvature correction, discussed above. Simulating the experiment with a Monte Carlo ray-tracing code yields for the width of the response function 22″ (FWHM), in reasonable agreement with the measurements. The additional broadening of the measured values is attributed to crystal imperfections, bending, and surface distortions. While the rocking curve widths are calculated to be 14.3″ and 12.9″ for the scandium $K\alpha_1$ and $K\beta_{1,3}$ lines, respectively [18], the Monte Carlo simulations show that over the angular range employed here, from 45° to 53°, the *total* resolution width varies by less than 1″. Thus, we consider the width of the response function to be constant for the range of angles employed in our measurements.

III. ATOMIC STRUCTURE CALCULATIONS

A. Introduction

The relativistic Dirac-Fock (DF) code GRASP of Dyall *et al.* [19] was employed for the *ab initio* calculations, supplemented by programs written in our laboratory. We have considered transitions involving up to two-vacancy states, of the forms $\underline{1s}\rightarrow\underline{np}$ and $\underline{1s3l}\rightarrow\underline{np3l}$ where $n=2,3$ for $K\alpha$ and $K\beta$, respectively, and $l=p$ or d. The first set of transitions is composed of the so-called diagram lines while the second is composed of the $\underline{3l}$-spectator vacancy satellites. The specific configurations employed for the diagram and satellite lines are discussed in Sec. IV.

B. Energy calculations

Previous studies [3,20] indicate that the excited atoms undergo rearrangement and a full relaxation before the x-ray emission occurs, at least far above the excitation threshold, which is the case in this study [21]. To reproduce this situation in the calculations we have generated in all cases the initial- and final-state wave functions and corresponding eigenenergies in two separate single-configuration runs where the wave functions and energies of *all* orbitals were allowed to vary.

The input to the code specifies the electronic occupation numbers of each shell in nonrelativistic notation, which are then expanded by the program to give all the corresponding

relativistic configurations, taking into account all possible couplings between the electrons in the open shells. The relativistic calculation is carried out in the jj coupling scheme and the results transformed back into the intermediate coupling scheme. The fully split array of the energy levels is calculated for the given configuration. Once the energy level array of the initial and final states is obtained, the transition energies are computed by taking the difference between appropriate pairs of energy levels, one from the initial-state array and one from the final-state array, as allowed by the electric dipole selection rules. This procedure yields the energies of all the lines of a multiplet resulting from transitions between states having specific initial and final electron occupations.

C. Line strength calculations

The GRASP code includes a facility for calculating the transition probabilities within a multiplet. This, however, is possible only when the wave functions of the initial and final states are orthogonal. In our case they are not, since they were generated in separate runs. We have used therefore configuration interaction calculations to obtain the various transition probabilities using once the wave functions of the initial state and, again, those of the final state. We find that for each multiplet studied here the two values for each line are within $\sim 10\%$ of each other, for all lines having a significant intensity. Thus, in the fits and figures of this study we use line strengths calculated from the initial state wave functions. We have verified that the use of final-state wave functions to calculate the line strengths has only a marginal effect on the various figures and plots presented here and no influence at all on our final conclusions.

D. Theoretical fits

A calculated multiplet is a ''stick diagram,'' consisting of a number of lines, each having a calculated height and energy, but a zero width. To fit the measured spectrum, each calculated line is represented by a Lorentzian and the spectrum is fitted by the following expression:

$$I_c(E)=\left[c_0+d_0E+\sum_{m=1}^{M} a_m \times\sum_{l=1}^{L} b_{lm}/\{1+[2(E-E_{lm}-\Delta_m)/\Gamma_{lm}]^2\}\right]\otimes G(E), \tag{1}$$

where c_0, d_0 define a linear background and $\Sigma_{m,l}$ sums over the different multiplets (m) and the lines within each multiplet (l). a_m and Δ_m are the relative intensity of each multiplet and the overall shift of its energy scale relative to the measured one, respectively. Both of these are common to all lines within a given multiplet. The shift Δ_m is required since the DF calculations are accurate to no better than a few eV [19] in absolute energy. Γ_{lm} are the full widths of the Lorentzians, representing the natural width of each line. To keep the number of fit variables manageable, all lines within a multiplet which lie below the midpoint between the $K\alpha_1$ and $K\alpha_2$ lines were assigned a common width, Γ_{m2}, as were those lying above the midpoint, Γ_{m1}. The only exception was the $1s3p\rightarrow 2p3p$ multiplet, where a clear division of the lines between the two ''parents'' $K\alpha_1$ and $K\alpha_2$ was not possible, and hence a common width was used for all its lines. E_{lm} and b_{lm} are the calculated energy and intensity of each line within the multiplet. The calculated model spectrum is convoluted ($\otimes$) by a unity-normalized Gaussian, $G(E)=(\sqrt{\ln 16/\pi}/w)\exp\{-[(E-E_{lm})\sqrt{\ln 16}/w]^2\}$, of full width at half maximum w, representing the instrumental resolution. For each multiplet the four parameters a_m, Δ_m, Γ_{m1}, and Γ_{m2} were allowed to vary in the fit. c_0, d_0, and w could also be varied in the fit, when needed. For the $K\beta_{1,3}$ spectrum an identical fit procedure was employed, except that a single width Γ_m was used for all lines of a multiplet, be it a diagram or a spectator one, for reasons discussed below.

IV. RESULTS AND DISCUSSION

A. Basic properties

To make a connection with previous studies of Sc as well as studies of other $3d$ transition metals, we now proceed to determine the basic properties of the measured spectra, and compare them with previously measured and calculated values. This is of particular interest, since our resolution is determined independently, and its effect on the spectra removed before calculating the parameters presented in the tables below.

1. $K\alpha_{1,2}$ spectrum

Two independent sets of measurements were carried out for the Sc $K\alpha$ spectrum. In the first, run I, a W-anode x-ray tube and crystal A were used. The most intense line of the primary radiation is the W $L\alpha_1$ at 8396 eV [15], well above the Sc K edge at 4492 eV [22]. The second measurement, run II, employed a Cr-anode x-ray tube and crystal B. The most intense lines here are the Cr $K\alpha_{1,2}$ at 5414 eV [15], about 20% higher than the Sc K edge.

We first discuss the results obtained in run I. Three separate measurements of the spectrum were performed to ensure reproducibility. The measured spectra were corrected as detailed above, summed, and converted to the proper energy scale. The total measurement statistics are indicated by the error bars in Fig. 3. To obtain the various quantities defining the raw spectrum, the discrete measured points were fitted by a sum of Voigt functions (VF), and the quantities derived from the fitted curve. The Voigt function, a convolution of a Lorentzian and a Gaussian, represents best the experimental situation where the Gaussian is the instrumental resolution function and the Lorentzian is the intrinsic line shape of a single transition line. Six VF's were required to obtain the best fit, three each for the $K\alpha_1$ and the $K\alpha_2$ lines. These VF's also correspond loosely to the three multiplets, listed in Table I, which contribute to each of the two lines. The full width at half maximum of the Gaussian was fixed in the fit at $w=0.45$ eV, as derived from the angular width of the pionic transition measurement, discussed above, and the dispersion $\Delta E/\Delta\theta=15.43$ meV/sec, corresponding to the Bragg angle of the $K\alpha_1$ transition. The measured raw data (points) are shown in Fig. 3, along with the six-VF fit (lines). The residu-

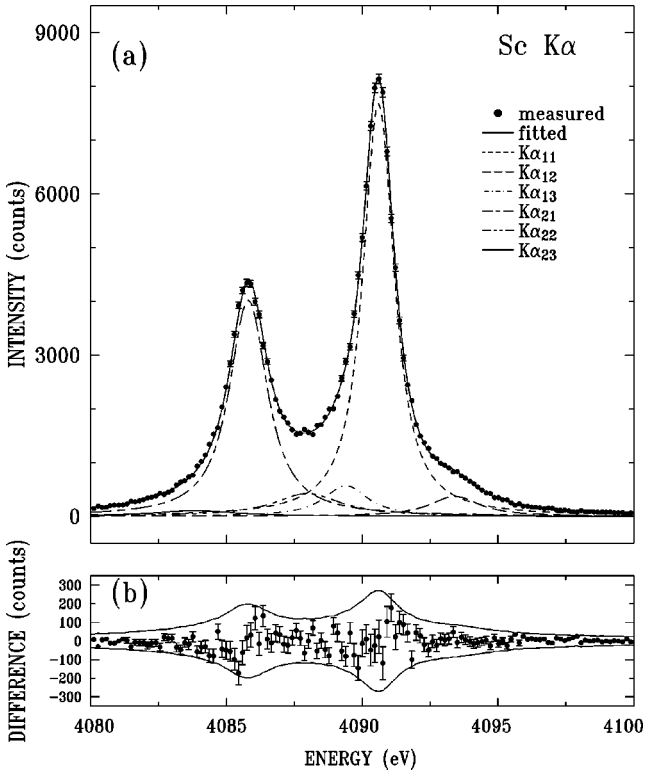

FIG. 3. The $K\alpha_{1,2}$ spectrum fitted by six Voigt functions (a) and the fit residuals (b). The individual Voigt functions in (a) are also shown. The lines in (b) denote the $\pm 3\sigma$ level of the spectrum, where σ is one standard deviation in each point due to counting statistics.

als in the lower panel are well below the $\pm 3\sigma$ levels (lines) of the measurement *everywhere*, demonstrating the high quality of the fit. Here σ is one standard deviation due to the counting statistics. The fit parameters and their approximate correspondence to specific transitions are summarized in Table I. The fit yields a value for the *reduced* χ^2 equal to 1.32, which is close to exhausting the measurements' accuracy at $\chi^2=1$. Since the basis for the six VF's fit is purely phenomenological, one should not attach too much physical significance to the specific values obtained for the widths, positions, etc., of the individual Lorentzians, although these numbers seem, in general, reasonable. The more physically motivated fit, based on *ab initio* atomic structure calculations, presented below, will allow doing so with a higher level of confidence. A fit with more than six VF's was also attempted, but the reduction obtained in the χ^2 was only marginal.

Using the six-VF representations, we have calculated the various properties of the spectrum, and summarized them in Table II, along with previous experimental values [23]. As can be observed, the agreement between our $K\alpha_1$ FWHM value and the width derived by Kawai *et al.* [10] from his measurements and by Pessa [24] from Parrat's measurements [9] is reasonable. In the case of the $K\alpha_2$ transition the FWHM derived by Pessa [24] is smaller than the our value and the value of Kawai *et al.* This may be due to overcorrection for resolution broadening in Ref. [24]. As the measured lines includes satellite contributions, they should appear broader in the experiment than the lifetime widths calculated for the pure diagram transition. Indeed, both our width and the width of Kawai *et al.* are significantly larger than the 1.03–1.09 eV obtained from the theoretical level widths calculations listed in Table VI, below. This is discussed further in conjunction with the *ab initio* fits below.

The asymmetry index of an x-ray emission line has been defined by Allison [25] as the ratio of the part of the FWHM lying to the low-energy side of the maximum ordinate to that on the high-energy side. While this is still the most commonly used definition for the asymmetry index [26,27], variations on this definition have also been used, differing in the way the peak position is determined. Following Kawai *et al.* [10] a general asymmetry index A_h may be defined as

$$A_h=\frac{(\text{low-}E\ \text{ side})}{(\text{high-}E\ \text{ side})}=\frac{f/2+x_h}{f/2-x_h}, \tag{2}$$

where f is the full width at half maximum, $x_h=a_h-b$, a_h is the nominal ''center'' determined as the half-width point's abscissa, when this width is taken at h% of the peak's height, and $b=a_{50}$ is the ''center'' position at 50% of the

TABLE I. Relative energy positions E_i, widths W_i, peak intensities I_i, and relative integrated intensities I_{int} obtained for the individual Voigt functions from a fit of the measured $K\alpha_{1,2}$ spectrum by a sum of six Voigt functions, as discussed in the text. The Gaussian resolution function had a full width at half maximum of 0.45 eV. The zero energy is the Sc $K\alpha_1$ peak energy, 4090.6 eV [15]. The numbers in parentheses correspond to one standard deviation due to the counting statistics. The *reduced* χ^2 value obtained for the fit is also shown.

Line	Transition	Designation	E_i (eV)	W_i (eV)	I_i (counts)	I_{int} (%)
			$\underline{K\alpha_1}$			
α_{11}	$\underline{1s}\rightarrow\underline{2p_{3/2}}$	Diagram $K\alpha_1$	0.000(4)	1.227(12)	8339(46)	50
α_{12}	$\underline{1s3p}\rightarrow\underline{2p_{3/2}3p}$	$K\alpha''$	2.815(40)	2.108(94)	383(10)	5
α_{13}	$\underline{1s3d}\rightarrow\underline{2p_{3/2}3d}$		−1.203(50)	1.82(16)	594(37)	5
			$\underline{K\alpha_2}$			
α_{21}	$\underline{1s}\rightarrow\underline{2p_{1/2}}$	Diagram $K\alpha_2$	−4.787(7)	1.552(21)	4245(31)	32
α_{22}	$\underline{1s3p}\rightarrow\underline{2p_{1/2}3p}$		−2.616(77)	2.93(43)	432(23)	6
α_{23}	$\underline{1s3d}\rightarrow\underline{2p_{1/2}3d}$		−6.74(17)	3.66(96)	108(8)	2
	Reduced χ^2		1.32			

TABLE II. Full widths at half maximum (FWHM), indices of asymmetry A_h, energy differences, and peak and integrated intensity ratios for the $K\alpha$ doublet, as derived from the fit of the spectrum using six Voigt functions (see text). Numbers in brackets are one-standard-deviation uncertainties in the last figure. $K\alpha^0_{1,2}$ denote the energy positions and intensities of the $K\alpha_{1,2}$ peaks. Previous measurements and theoretical values are also shown.

Source	$K\alpha_1$			$K\alpha_2$		Energy differences (eV)		Intensity ratios (%)	
	FWHM (eV)	A_{100}	A_{90}	FWHM (eV)	A_{100}	$K\alpha^0_1$-$K\alpha^0_2$	$K\alpha''$-$K\alpha^0_1$	Peak $K\alpha^0_2/K\alpha^0_1$	Integrated $K\alpha''/K\alpha_1$
This work									
Run I	1.332(16)	1.113(17)	1.082(7)	1.744(28)	0.884(16)	4.784(8)	2.809(34)	52.1(5)[f]	6.3(5)[h]
								50.9(5)[g]	
Run II	1.389(95)	1.133(53)	1.122(49)	1.770(75)	0.910(25)	4.772(13)	2.95(10)	49.3(3.0)[f]	6.9(7)[h]
Kawai *et al.*[a]	1.446(12)		1.175(20)	1.779(40)		4.768(15)			
Parratt[b]	1.28			1.51			3.0		1.4
Bearden[c]						4.5			
Scott[d]							2.8		
Salem and Wimmer[e]								50.7(1.0)	

[a]Reference [10]. The asymmetry given in the original paper is a misprint.
[b]Reference [9]. Widths as calculated from Parratt's data by Pessa [24].
[c]Reference [15].
[d]Reference [8].
[e]Reference [30].
[f]Ratio of the peak intensities, $K\alpha^0_2/K\alpha^0_1$ of the full fit to the data.
[g]Ratio of the peak intensities, $K\alpha^0_{21}/K\alpha^0_{11}$, of the Lorentzians representing the ''diagram'' lines.
[h]The integrated $K\alpha_1$ intensity is assumed to be the 2/3 of the total $K\alpha$ intensity.

full height. For $h=100$, a_{100} is the position of the peak and the corresponding index of asymmetry, A_{100}, is the conventional one defined by Allison [25]. When $x_h \geqslant 0$, which occurs when a_h is on the high-energy side of b, $A_h \geqslant 1$ while $x_h < 0$ yields $A_h < 1$.

The asymmetry indices obtained for the $K\alpha_1$ and $K\alpha_2$ lines are given in Table II. A_{90} allows a direct comparison with the values of Kawai *et al.* [10], the only ones published for scandium. Our indices are greater than unity for $K\alpha_1$ but smaller than unity for $K\alpha_2$. The $K\alpha_1$ value is significantly lower than that of Kawai *et al.* However, this value is very sensitive to the shape and width of the experimental resolution function. While our A_{90} is obtained from the resolution-corrected spectrum, that of Kawai *et al.* was not. Our raw, resolution-uncorrected data yields, for $K\alpha_1$, $A_{90}=1.14$, less than two standard deviations from the value of Kawai's *et al.*

The $A_h<1$ of $K\alpha_2$ is mainly due to the large contribution to the intensity on the high-energy side of this line from the low-energy wing of the strong $K\alpha_1$ line. This distortion effectively prevents the extraction of an intrinsic asymmetry parameter for the $K\alpha_2$ line. By the same token, the corresponding increase in the intensity of the low-energy wing of the $K\alpha_1$ line due to contributions from the $K\alpha_2$ line probably increases the asymmetry parameter derived for $K\alpha_1$ from the measured spectrum beyond its intrinsic value.

Turning now to the measured lines' *peak* positions, $K\alpha^0_1$ and $K\alpha^0_2$, we note that $K\alpha^0_1$ is found to be (-0.007 ± 0.004) eV lower than the centroid of the $K\alpha_{11}$ component, representing the diagram transition. This point is of importance when correlating the peak position with the diagram transition's energy. The spin doublet splitting $K\alpha^0_1$-$K\alpha^0_2$ was found to be (4.784 ± 0.008) eV. Kawai *et al.* obtained (4.768 ± 0.015) eV, determining the position of the $K\alpha_1(K\alpha_2)$ line from the center point at 90% intensity of the corresponding $K\alpha_1(K\alpha_2)$ complex. Following the method of Kawai *et al.* method we find (4.779 ± 0.013) eV, in good agreement with Kawai *et al.* Photoelectron spectroscopic measurements yield a $2p$ spin doublet splitting of (4.93 ± 0.1) eV for metallic Sc [28,29], again, in good agreement with our value. Bearden's [15] lower value of 4.5 eV might have been obtained on a nonmetallic sample, as done by Parratt [9], who employed Sc_2O_3 rather than metallic Sc in his measurements. The $K\alpha^0_1$-$K\alpha^0_2$ splitting is sensitive to the valence state of the atom and the value of (4.33 ± 0.01) eV obtained by Kawai *et al.* for Sc_2O_3 [10] is indeed closer to Bearden's value than to those of the pure metal.

The *integrated* intensity ratio $I_{int}(K\alpha_2)/I_{int}(K\alpha_1)$ is, in principle, a highly important measurable. It yields the relative $K\alpha_2/K\alpha_1$ transition probability, a quantity calculated in and used to test many theoretical models. However, its determination from the spectrum measured here is not feasible due to the partial overlap between the $K\alpha_1$ and $K\alpha_2$ lines. Nevertheless, it is possible to determine the *peak* intensity ratio $I(K\alpha^0_2)/I(K\alpha^0_1)$ from the six-Lorentzian fit to our data. This yields $(52.1 \pm 0.5)\%$, which agrees with Salem and Wimmer's [30] $(50.7 \pm 1)\%$. Salem and Wimmer's value was, however, calculated after correcting each measured peak value for the contribution from the underlying tail of the adjacent line. This corresponds in our fit to the peak intensity ratio $I(K\alpha^0_{21})/I(K\alpha^0_{11})$ of the Lorentzians representing the ''diagram'' lines. Indeed, our fit yields $I(K\alpha^0_{21})/I(K\alpha^0_{11})=(50.9 \pm 0.5)\%$, in excellent agreement with Salem and Wimmer.

Since the $K\alpha''$ satellite does not appear as a well-separated line, the uncertainties in the determination of its parameters from the measured data are larger than those of

the $K\alpha$ lines. The $K\alpha''$-$K\alpha_1^0$ energy separation of 2.809 ± 0.034 eV from our fit is slightly smaller than the 3 eV measured by Parratt, and is in very good agreement with the Hartree-Fock calculations of Scott [8] which yields a 2.8 eV separation for the main component of the corresponding $\underline{3p}$-spectator multiplet. Our $I_{int}(K\alpha'')/I_{int}(K\alpha_1)$ integrated intensity ratio of $(6.3\pm 0.5)\%$ (see Table II) is more than fourfold larger than Parratt's value [9]. This large discrepancy is partly due to the different method of determination of this quantity. However, Parratt's use of Sc_2O_3 rather than the metallic Sc used here should contribute considerably to this difference. As observed in Fig. 1 of Ref. [10], the $K\alpha''$ feature is more prominent in metallic Sc than in any of its compounds. This happens because in the case of Sc_2O_3 the Sc $3p$ electrons form molecular orbitals with the O $2s$ electrons [10]. Thus, once a $\underline{3p}$ spectator hole is created, it is more likely to be depopulated faster in Sc_2O_3, where nearby ligand electron are available, than in metallic Sc where the $3p$ orbitals are less delocalized and no such electrons are easily available.

Finally, we discuss the results obtained in run II. The spectrum was fitted with six VF's, in which the FWHM of the Gaussian instrumental resolution width was fixed at 0.40 eV, according to the measured resolution of the B crystal. The fit yields a χ^2 of 0.9. The various quantities extracted from the spectrum are summarized in Table II. The higher uncertainties obtained here, relative to those of run I, are due to the poorer counting statistics. The results obtained in the two runs are seen to be within one standard deviation from each other, and thus, run II supports all the results and conclusions of run I.

2. $K\beta_{1,3}$ spectrum

The scandium $K\beta_{1,3}$ spectrum was measured using Cr-anode x-ray tube excitation and the B crystal. It is shown in Fig. 4, along with a fit to a sum of Voigt functions as done for the $K\alpha_{1,2}$ spectrum. The lines of this spectrum overlap considerably more than those of the $K\alpha_{1,2}$ one. Six VF were sufficient to fit the spectrum very well ($\chi^2=1.15$). The fit employed, as discussed above, a Gaussian resolution of 0.57 eV (FWHM) obtained from the $\pi Ne(6h\rightarrow 5g)$ transition for this energy. The dispersion at the Bragg angle corresponding to the $K\beta_{1,3}$ peak was $\Delta E/\Delta\theta=22.136$ meV/sec. The parameters defining the six VF's, and the corresponding transitions, are listed in Table III.

In contrast to the $K\alpha_{1,2}$ spectrum, where the fitted individual VF's could be correlated roughly with the various electronic transitions, those of the $K\beta_{1,3}$ spectrum cannot, and are, therefore, purely phenomenological. There are only two probable exceptions. One is the dominant $K\beta_A$ line. Its width is 1.04 ± 0.04 eV, while the expected spin doublet $K\beta_1$-$K\beta_3$ energy splitting is less than 0.5 eV in atomic Sc [15,29,31]. Thus, the $K\beta_A$ line can be cautiously attributed to the ''diagram'' $K\beta_{1,3}$ transitions. The other exception is the $K\beta_F$ line, which clearly corresponds to the $K\beta''$ feature.

The widths, asymmetries, etc., derived from the spectrum are listed in Table IV. They have been extracted both directly from the measured raw spectrum, and from the resolution corrected spectrum, using the six VF representation of Fig. 4. In contrast to the $K\alpha_{1,2}$ spectrum, the diagram line overlap

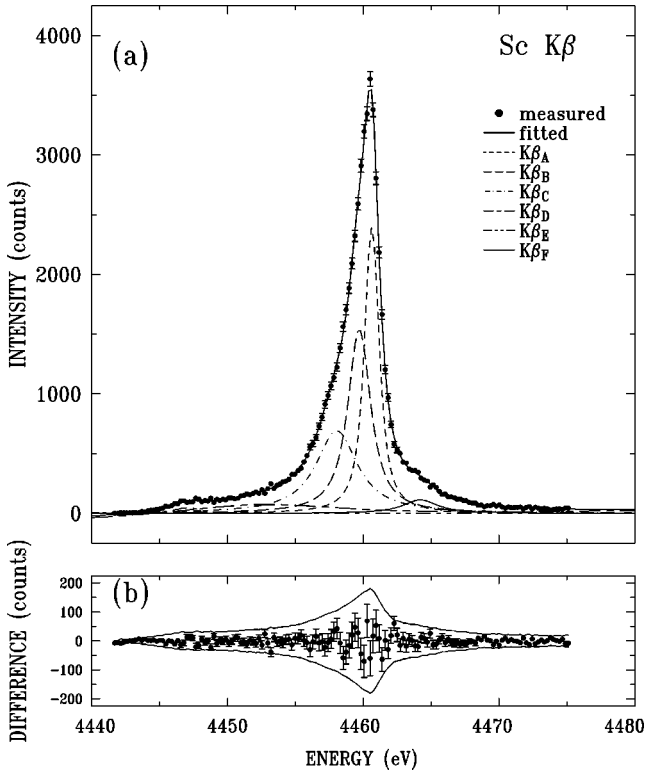

FIG. 4. The $K\beta_{1,3}$ spectrum fitted by 6 Voigt functions (a) and the fit residuals (b). The individual Voigt functions in (a) are also shown. The lines in (b) denote the $\pm 3\sigma$ level of the spectrum, where σ is one standard deviation in each point due to counting statistics.

does not allow to extract here meaningful ''lifetime'' widths that can be compared directly with calculated lifetime widths of individual transition lines. This is done below for the fits of the *ab initio* calculated spectrum. We note, however, that our raw FWHM width is in good agreement with that of Kawai *et al.* [10] (uncorrected) value. The resolution-corrected value is, however, significantly lower.

The A_{100} values obtained with and without the resolution correction differ significantly, as expected, demonstrating the importance of the experimental resolution correction, especially for strongly asymmetric lines, as is the present one. For the Sc A_{100} index no other experimental determination is available in the literature, to the best of our knowledge. However, for the neighboring elements, titanium ($Z=22$) and vanadium ($Z=23$), the $K\beta_{1,3}$ (raw) A_{100} index is 1.73 and 1.50, respectively [26], while for scandium ($Z=21$) we obtain 1.98. it is not clear whether these differences reflect intrinsic differences in the emission process or the atomic structure among these elements or are just artifacts due to different experimental procedures and data analysis methods, metal and nonmetal target differences, etc. The difference between the A_{66} indices obtained from the raw and the corrected spectra is significantly lower than for A_{100} since the upper part of the emission line is more symmetric and thus less sensitive to distortions caused by, e.g., finite experimental resolution. Our A_{66} values are, again, in good agreement with those of Kawai *et al.*

Finally, the $K\beta''$-$K\beta_{1,3}^0$ splitting and the integrated intensity ratio $I_{int}(K\beta'')/I_{int}(K\beta_{1,3})$ are also listed in Table IV.

TABLE III. Relative energy positions E_i, widths W_i, peak intensities I_i, and relative integrated intensities I_{int} obtained for the individual Voigt functions from a fit of the measured $K\beta_{1,3}$ spectrum by a sum of six Voigt functions, as discussed in the text. The Gaussian resolution full width at half maximum used in the fit was 0.57 eV. The zero-energy position is the energy of the Sc $K\beta_{1,3}$ peak, 4460.5 eV [15]. Numbers in parentheses correspond to one standard deviation uncertainties in the last digit due to counting statistics. The *reduced* χ^2 value obtained for the fit is also shown.

Line	Transition	Designation	E_i (eV)	W_i (eV)	I_i (counts)	I_{int} (%)
β_A	$\underline{1s}\rightarrow\underline{3p_{1/2,3/2}}$	Diagram $K\beta_{1,3}$	0.00(1)	1.04(4)	2809(43)	28
β_B			−0.93(2)	1.85(10)	1639(36)	30
β_C			−2.59(3)	3.60(14)	704(14)	24
β_D			−8.30(11)	16.49(72)	120(2)	14
β_E			−13.58(12)	2.20(60)	48(5)	1
β_F	$\underline{1s3p}\rightarrow\underline{3p3p}$	$K\beta''$	3.58(10)	2.99(46)	115(6)	3
	Reduced χ^2		1.15			

Unfortunately, to the best of our knowledge, no other measured values are available for these quantities. We note, however, that the obtained value of $(3.5\pm0.5)\%$ for the integrated intensity ratio $I_{int}(K\beta'')/I_{int}(K\beta_{1,3})$ is very close to the value of $(4.2\pm0.5)\%$ obtained for the $I_{int}(K\alpha'')/I_{int}(K\alpha_{1,2})$ integrated intensity ratio [see last column in Table II, with $I_{int}(K\alpha_{1,2})\approx(3/2)I_{int}(K\alpha_1)$].

B. Comparison with theory

1. $K\alpha_{1,2}$ spectrum

a. Calculated multiplets. As in previous studies [3], we carried out *ab initio* relativistic Dirac-Fock calculations for transitions between selected initial- and final-state electronic configurations. All calculations were done assuming full relaxation between the excitation (i.e., the $1s$ electron ejection) and deexcitation (the filling of the $\underline{1s}$ hole by a higher-shell electron and the emission of an x ray) processes, as detailed above. The electronic configuration of the neutral scandium atom is nominally $[\mathrm{Ar}]3d^14s^2$ (denoted below by g_1). However, the $3d$ and $4s$ are valence shells and have small energy separations (a fraction of 1 eV [32]), so that the probability of having the outer three electrons distributed differently from the nominal within these shells may not be negligible *a priori*. Hence, we carried out calculations, for both the diagram and satellite lines, assuming several different ground-state configurations of the outer electrons. Only one- and two-electron transitions (i.e., diagram and one-spectator transitions) were considered, as was the case for Cu [3]. As we show below, these were sufficient to account for the line shapes of the $K\alpha$ spectrum, and invoking lower-probability, three-electron transitions was not required.

The calculated ''stick diagrams'' of the various calculated transition multiplets are given in Fig. 5, marked with the corresponding outer electron configurations, for the diagram, the $\underline{3d}$- and the $\underline{3p}$-spectator transitions. The measured spectrum and a ''stick diagram'' derived from the phenomenological six-VF fit discussed above are also shown. Frame (c) shows the diagram transitions for the nominal g_1 ground state configuration, with a single $\underline{1s}$ hole in the initial state and a single $\underline{2p}$ hole in the final state. The general alignment of the measured and calculated spectra is good, given the 1–2 eV absolute energy accuracy of the calculations. The large number of lines, 36 in all, is due to the fact that there are two open shells ($\underline{1s}$ or $\underline{2p}$ plus $3d^1$). The general shape of the calculated spectrum closely follows the measured one and, although shifted, that of the phenomenological spectrum in (b). Removing one or both $4s$ electrons (d), (e) leaves the calculated spectrum virtually unchanged in both overall shape and energy position, as was also observed for Cu [3]. Even more drastic changes, like pulling one $4s$ electron into the $3d$ shell and removing the other (f) have only little influence on the spectral shape. The $\underline{3d}$-spectator spectrum (g) is, however, considerably different; there are now two lines only, and the spectrum is slightly ($\sim$2 eV) downshifted relative to the measured peaks. Finally, (h) and (i) show the

TABLE IV. Full widths at half maximum (FWHM), indices of asymmetry A_h, energy differences, and integrated intensity ratios for the $K\beta$ doublet, as derived from the fit of the spectrum using six Voigt functions (see text). Numbers in parentheses are one-standard-deviation uncertainties in the last figure. $K\beta^0_{1,3}$ denotes the energy position of the $K\beta_{1,3}$ peak. Previous measurements are also shown.

		$K\beta_{1,3}$		Energy difference (eV)	Integrated intensity ratio (%)
Source	FWHM (eV)	A_{100}	A_{66}	$K\beta''$-$K\beta^0_{1,3}$	$K\beta''/K\beta_{1,3}$
This work					
Resolution-corrected spectrum	2.15(6)	2.38(12)	1.38(5)	3.64(10)	3.5(5)
Raw data	2.45	1.98	1.34		
Kawai *et al.*	2.438(25)		1.398(24)		

[a]Reference [10].

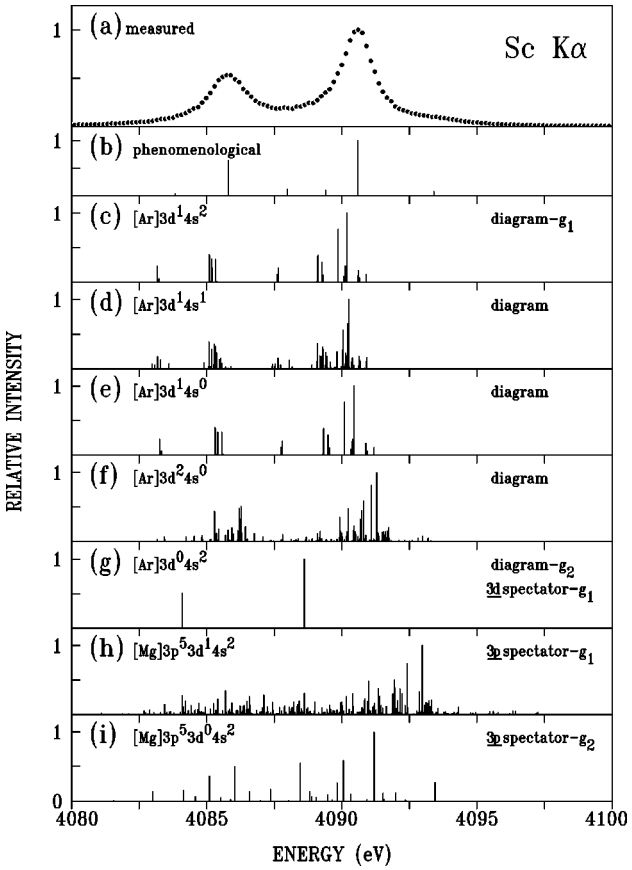

FIG. 5. The $K\alpha_{1,2}$ measured spectrum (a), phenomenological fit of Fig. 3 (b), and *ab initio* calculated multiplets (c)–(i) for the indicated electronic configurations and transitions. In all frames, the height of individual lines represents the *integrated* intensity of that transition, normalized to the most intense line of the multiplet.

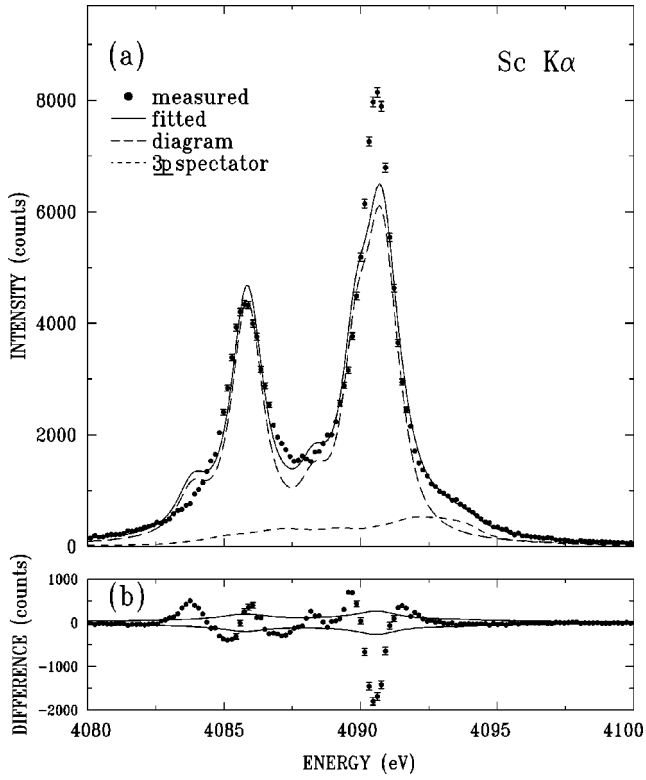

FIG. 6. Fit of the measured $K\alpha_{1,2}$ spectrum by the nominal diagram multiplet (c) and $3\underline{p}$-spectator multiplet (h) in Fig. 5. The individual multiplet contributions are shown in (a). The residuals and $\pm 3\sigma$ levels are shown in (b). The fit parameters are listed in Table V under ''Fit A.''

$3\underline{p}$-spectator transitions assuming the nominal $g_1([\mathrm{Ar}]3d^14s^2)$ and the $[\mathrm{Ar}]3d^04s^2$ (denoted g_2) ground states, respectively. For the nominal ground state g_1 the strongest lines of the calculated $3\underline{p}$-spectator multiplet (h) are well aligned with the measured $K\alpha''$ feature, and it has the right shape: strong lines near 4093 eV and a broad and low background over the rest of the range. This supports, therefore, the assignment of $K\alpha''$ to this transition, originally proposed by Druyvesteyn [4] as early as 1928, and supported by Parratt's measurements [9], the Hartree-Fock calculations of Scott [8], and the study of Kawai *et al.* [10]. The $3\underline{p}$-spectator for the $3d$-depleted ground state g_2 (i) is less well aligned with $K\alpha''$, although the strongest line is still within $\sim$2.5 eV of it.

b. Theoretical fits. The minimal set of multiplets that can possibly contribute to the $K\alpha$ spectrum includes the diagram transitions and, because of the clear identification of the $K\alpha''$ feature, the $3\underline{p}$-spectator one. A fit employing these two multiplets for the nominal atomic electron configuration, namely, (c) and (h) in Fig. 5, is shown in Fig. 6, and the parameters obtained in the fit listed in Table V under ''Fit A.'' The poor quality of the fit, indicated by the large fit residuals in Fig. 6(b), shows that a diagram and a $3\underline{p}$-spectator transition are insufficient to explain the line shape. Attempts to use the same combination with other ''diagram'' transitions, namely, (d), (e), and (f) in Fig. 5, yield almost identical results. It is clear, therefore, that contributions from additional multiplets must be included. Note that even for this poor fit a $\sim$14% contribution by the $3\underline{p}$-spectator transition is indicated. The more loosely bound $3\underline{d}$ spectator, which should have a higher excitation probability, should contribute significantly more to the spectrum. Thus, a fit including multiplets (c), (g), and (h) in Fig. 5 was carried out, with results shown in Fig. 7, and parameters listed in Table V under ''Fit B.'' Although discrepancies still exist [see Fig. 7(b)], this combination yields a considerably better fit to the measured spectrum than the previous choice. In fact, attempts to improve the fit by including the same three transitions, but using different ''diagram'' transitions [e.g., (d) or (e)], resulted in worse fits than that shown in Fig. 7.

Computationally, the ''two-lines-only'' structure of the $3\underline{d}$-spectator multiplet is a decisive factor in obtaining a good fit to the sharp measured peaks in Fig. 7. A similar two-line diagram multiplet is also obtained if a ground-state configuration $[\mathrm{Ar}]3d^04s^2$, or even $[\mathrm{Ar}]3d^04s^0$, is assumed. Given such a ground-state configuration, would it be possible to obtain a good fit using only that diagram and the $3\underline{p}$-spectator multiplet? Note that on physical grounds such a ground state will not be entirely unreasonable, since while in an isolated atom the $3d$ orbital is reasonably sharp, in the solid-state-bound atom the $3d$ orbital is more diffuse and molecular like [10,33]. To answer this question a new fit, using multiplet (g) as the ground state g_2 and (i) as the corresponding $3\underline{p}$-spectator multiplet, was carried out with the results shown in Fig. 8, and the fit parameters listed in Table

TABLE V. Fit results for the $K\alpha$ scandium spectrum. g_1 and g_2 denote the ground-state electronic configurations $[\mathrm{Ar}]3d^14s^2$ and $[\mathrm{Ar}]3d^04s^2$, respectively. Δ, Γ, a_m, and I_{int} denote the shift, width, amplitude, and integrated intensity of each multiplet (see text). For multiplets that were divided into two parts, two widths are listed. $|C+DE|$ (where E is in eV) is the background and w is the full width at half maximum of the Gaussian representing the instrumental resolution function. Reduced χ^2 of the fits are also shown.

Parameters	Ground state	Transitions	Fit A (Fig. 6)	Fit B (Fig. 7)	Fit C (Fig. 8)
Δ (eV)	g_1	$\underline{1s}\rightarrow\underline{2p}$	0.65(2)	0.43(1)	
	g_2	$\underline{1s}\rightarrow\underline{2p}$			1.87(1)
	g_1	$\underline{1s3d}\rightarrow\underline{2p3d}$		2.02(1)	
	g_1	$\underline{1s3p}\rightarrow\underline{2p3p}$	0.80(1)	0.80(1)	
	g_2	$\underline{1s3p}\rightarrow\underline{2p3p}$			0.06(5)
Γ (eV)	g_1	$\underline{1s}\rightarrow\underline{2p_{3/2}}$	0.94(2)	1.06(2)	
	g_1	$\underline{1s}\rightarrow\underline{2p_{1/2}}$	1.14(2)	1.06(2)	
	g_2	$\underline{1s}\rightarrow\underline{2p_{3/2}}$			1.08(2)
	g_2	$\underline{1s}\rightarrow\underline{2p_{1/2}}$			1.39(2)
	g_1	$\underline{1s3d}\rightarrow\underline{2p_{3/2}3d}$		0.80(2)	
	g_1	$\underline{1s3d}\rightarrow\underline{2p_{1/2}3d}$		1.30(4)	
	g_1	$\underline{1s3p}\rightarrow\underline{2p3p}$	1.18(8)	1.15(4)	
	g_2	$\underline{1s3p}\rightarrow\underline{2p_{3/2}3p}$			1.69(4)
	g_2	$\underline{1s3p}\rightarrow\underline{2p_{1/2}3p}$			1.60(8)
a_m (counts)	g_1	$\underline{1s}\rightarrow\underline{2p}$	2662(36)	1397(17)	
	g_2	$\underline{1s}\rightarrow\underline{2p}$			17 413(200)
	g_1	$\underline{1s3d}\rightarrow\underline{2p3d}$		12 294(183)	
	g_1	$\underline{1s3p}\rightarrow\underline{2p3p}$	69(4)	78(2)	
	g_2	$\underline{1s3p}\rightarrow\underline{2p3p}$			1160(23)
C			$-10\,873(16)$	$-13\,732(3)$	$-7789(4)$
D			2.65(1)	3.35(1)	1.90(1)
w (eV)			0.45	0.45	0.45
I_{int} (%)	g_1	$\underline{1s}\rightarrow\underline{2p}$	86	47	
	g_2	$\underline{1s}\rightarrow\underline{2p}$			65
	g_1	$\underline{1s3d}\rightarrow\underline{2p3d}$		38	
	g_1	$\underline{1s3p}\rightarrow\underline{2p3p}$	14	15	
	g_2	$\underline{1s3p}\rightarrow\underline{2p3p}$			35
Reduced χ^2			27.85	7.35	11.97

V under ''Fit C.'' While now the ''bump'' at 4083 eV does not appear, the overall quality of the fit is clearly inferior to fit B in Fig. 7, as observed by inspection of the corresponding fits and residuals. The basic problem here is that the removal of the $3d$ electron reduces slightly, but significantly, the $2p_{1/2}$-$2p_{3/2}$ spin doublet splitting, making it smaller than the observed $K\alpha_1$-$K\alpha_2$ energy separation.

The discussion so far was based on an eye inspection of the figures showing the various fits. The reduced χ^2 values in Table V quantify the relative quality of each fit. For fit A, which includes the diagram plus the $\underline{3p}$-spectator transitions only, with the nominal $g_1([\mathrm{Ar}]3d^14s^2)$ ground state, a $\chi^2 \approx 28$ is obtained. Using different ground state electron configurations, namely, $[\mathrm{Ar}]3d^14s^1$ and $[\mathrm{Ar}]3d^14s^0$, yields similar values. Fit C, employing the $g_2([\mathrm{Ar}]3d^04s^2)$ ground state and the corresponding $\underline{3p}$ spectator only, reduces χ^2 to ~ 12, less than half of fit A. While this is a significant improvement, the fit is still not good, as discussed above. Returning now to the nominal electron configuration, and adding the $\underline{3d}$-spectator transition (fit B), results in a further reduction to $\chi^2 = 7.35$. The conclusion emerging from both the χ^2 values and the inspection of Figs. 6–8 is that the inclusion of the $\underline{3d}$ spectator is mandatory to obtain a good fit, and that the use of the nominal ground state g_1 and the three transitions, the diagram and the $\underline{3p}$ and $\underline{3d}$ spectators, are sufficient to account well, quantitatively, for the measured line shapes of the $K\alpha$ spectrum.

c. Spectral characteristics obtained from the fit. We now discuss the parameters obtained from the best fit, fit B in Table V, and compare them, where relevant, with other available data.

The natural widths obtained are listed in Table VI, along with several previous theoretical and semiempirical values. As a separation of the measured spectra into individual multiplet contributions was not attempted in any of the previous measurements, experimentally derived widths, which belong

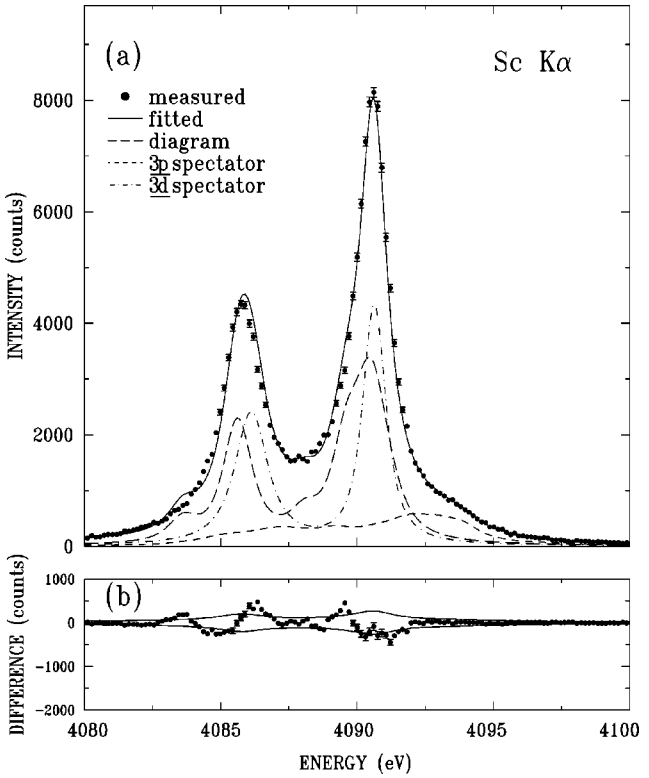

FIG. 7. Fit of the measured $K\alpha_{1,2}$ spectrum by the nominal diagram multiplet (c), $3p$-spectator multiplet (h), and the $3d$-spectator multiplet (g) in Fig. 5. The individual multiplet contributions are shown in (a). The residuals and $\pm 3\sigma$ levels are shown in (b). The fit parameters are listed in Table V under ''Fit B.''

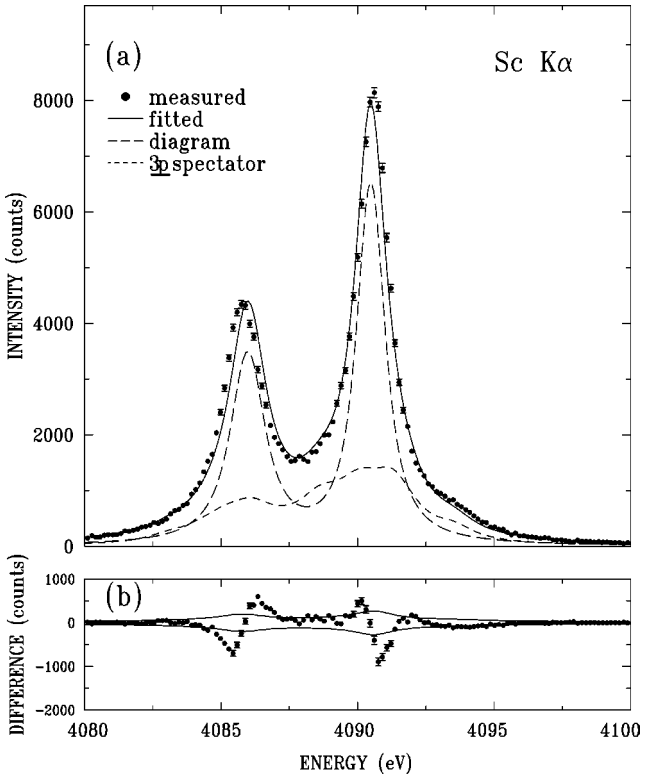

FIG. 8. Fit of the measured $K\alpha_{1,2}$ spectrum by the $3d$-spectator multiplet (g) and the $3p$-spectator multiplet (i) in Fig. 5. The individual multiplet contributions are shown in (a). The residuals and $\pm 3\sigma$ levels are shown in (b). The fit parameters are listed in Table V under ''Fit C.''

to the composite lines, were not included in the table. The agreement of the theoretical widths with those obtained from fit B is excellent: $\lesssim 4\%$. By contrast, the linewidths derived from the resolution-corrected spectrum, *before* the removal of the spectator contributions, in Table II overestimate significantly the theoretical and spectator-removed widths in Table VI. This demonstrates the importance of properly removing the contributions of the spectator transitions to the line shape for obtaining a meaningful comparison with theoretical calculations. Note also that the widths obtained from the two other fits in Table V are in a much worse agreement with theory. This supports further the conclusion above that the inclusion of the $3d$ spectator is mandatory to account for the shape of the $K\alpha$ spectrum.

The integrated intensities obtained from fit B indicate that the $3d$ spectator's contribution is about equal to that of the diagram line: $\sim 38\%$ of the total intensity of the $K\alpha_{1,2}$ lines. While this is higher than the 30% obtained for Cu [3], such an increase is not unreasonable in view of the lower atomic number of Sc and the concomitantly lower $3d$ binding energy, only 0.8 eV as compared to 2.8 eV in Cu [32]. A large increase is also observed in the $3p$-spectator intensity: 15% in Sc vs 0.5% in Cu [3], presumably for the same reason. This value for Sc greatly exceeds the 1.4% estimate of Parratt [9] for the corresponding $K\alpha''$ feature. The true difference is even larger, since Parratt's value is relative to the $K\alpha_1$ line, while the present value is a percentage out of the total $K\alpha_{1,2}$ line spectrum. Parratt's estimate, however, was calculated by taking the excess intensity in the $K\alpha''$ feature over the smoothly falling wing of the diagram line. This leaves out almost all of the intensity of the multiplet, which lies mostly under the $K\alpha_1$ and $K\alpha_2$ peaks, as shown in Fig.

TABLE VI. Full widths at half maximum, in eV, obtained from the best fit of the theoretical DF-calculated spectra to the measured one (''present'') and several theoretical and semiempirical calculations.

	FWHM (eV)			
Source	$K\alpha_1$	$K\alpha_2$	$K\beta_1$	$K\beta_3$
Present				
Best theoretical fit	1.06(2)	1.06(2)	2.8(12)	2.8(12)
Theoretical				
McGuire[a]	1.09	1.09		0.971
Chen and co-workers[b]	1.08		1.082	1.082
Crasemann and Chen[c]	1.028	1.026	0.850	0.859
Semiempirical				
Krause and Oliver[d]	1.05	1.06		
Perkins *et al.*[e]	1.03	1.03	0.85	0.86

[a]*K*-level width from Ref. [41], *L*- and *M*-level widths linearly interpolated from Refs. [42] and [43], respectively.
[b]*K*-, *L*-, and *M*-level widths linearly interpolated from Refs. [44], [45], and [46], respectively.
[c]*K*-, *L*-, and *M*-level widths from Ref. [35].
[d]From Ref. [47].
[e]From Ref. [48].

TABLE VII. Measured and theoretical $K\alpha_1$-$K\alpha_2$ spin doublet splitting, in eV. The theoretical ''Present'' values were calculated using multiplets (c) and (g) in Fig. 5 and a Lorentzian lifetime width of 1.06 eV (Table VI) for all transitions.

Source	$E_{K\alpha_1}$-$E_{K\alpha_2}$ (eV)
Theoretical	
Present DF: $[\mathrm{Ar}]3d^14s^2$	4.86
$[\mathrm{Ar}]3d^04s^2$	4.50
Kuhn and Scott[a]	4.46
Measured	
Present (metal)	4.87(1)
Kawai *et al.*[b] (metal)	4.77(1)
Kawai *et al.*[b] (compounds)	4.33–4.48
Bearden [c]	4.55

[a]Reference [49]. This value is the splitting of the strongest lines of the calculated multiplet.
[b]Reference [10].
[c]Reference [15].

7. The same holds for the phenomenological six-VF fit discussed above, even though the value derived there is somewhat closer to the present 15% value.

The $K\alpha_1$-$K\alpha_2$ spin doublet splitting, obtained from our DF calculations and measurements, as well as those from several other theoretical and experimental sources, are summarized in Table VII. The agreement between the present measurement and that of Kawai *et al.* [10] for metallic scandium is very good, while the compounds studied by them all show smaller splittings. Bearden's 4.55 eV is lower than our values and those of Kawai *et al.* for metallic Sc, and thus seems to have been measured also on a compound, possibly an oxide, as were Parratt's measurements [9]. The DF calculations show a decreasing trend in the splitting with decreasing $3d$ shell population. The $[\mathrm{Ar}]3d^14s^2$ fine structure splitting value is in excellent agreement with the measured metallic sample value, while that of $[\mathrm{Ar}]3d^04s^2$ is lower and very close to the splittings observed by Kawai *et al.* in the compounds. These correspondences seem to indicate that for the metallic Sc the single $3d$ electron of the nominal Sc configuration is atomically localized, while for the compounds the $3d$ atomic level is depopulated, the $3d$ electron going presumably into the molecular bonding orbitals. From a comparison of the measured $K\alpha_1$ chemical shift with DV-Xα molecular structure calculations Kawai *et al.* [10] conclude similarly that the formation of the chemical bond depopulates the $3d$ shell.

Finally, the contribution of $\underline{3s}$-spectator transitions are negligible for the spectra discussed in this work, as was also found for Cu [3]. This is due to the lower cross section for the formation of a vacancy in these more strongly bound shells, the lower number of electrons in the s shell as compared to the p shell, and, more significantly, the strong Coster-Kronig transitions which depopulate such vacancies very fast [34], as demonstrated by the large natural width of the $3s$ level, 4.59 eV, as compared with the much narrower widths, 0.23 eV, of the $3p$ levels [35].

2. $K\beta_{1,3}$ spectrum

a. Calculated multiplets. DF calculations, identical with those discussed above for $K\alpha_{1,2}$ except for the obvious replacement of the active $2p$ electron with the $3p$ one, were carried out for the $K\beta_{1,3}$ spectrum as well. The calculated ''stick diagram'' multiplets are shown in Fig. 9, along with the measured spectrum and the phenomenological six-VF fit. The general alignment of the diagram multiplets (c)–(f) with the measured spectrum is inferior to that of the $K\alpha_{1,2}$ spectrum, although still within the few-eV accuracy limit of the *ab initio* DF calculations. The conclusions on the relative unimportance of the $4s$ shell population and the strong influence of the removal of the $3d$ electron on the spectral shape, obtained above for $K\alpha_{1,2}$, hold true here as well, as observed in frames (c)–(g). The positions of the $\underline{3p}$-spectator multiplets (h)–(i) on the high-energy side of the strongest lines in the corresponding ''diagram'' multiplets (c)–(g) correspond very well with the position of the $K\beta''$ feature (at ~4464 eV) relative to the $K\beta_{1,3}$ peak, supporting a suggested [10] assignment of $K\beta''$ to this transition.

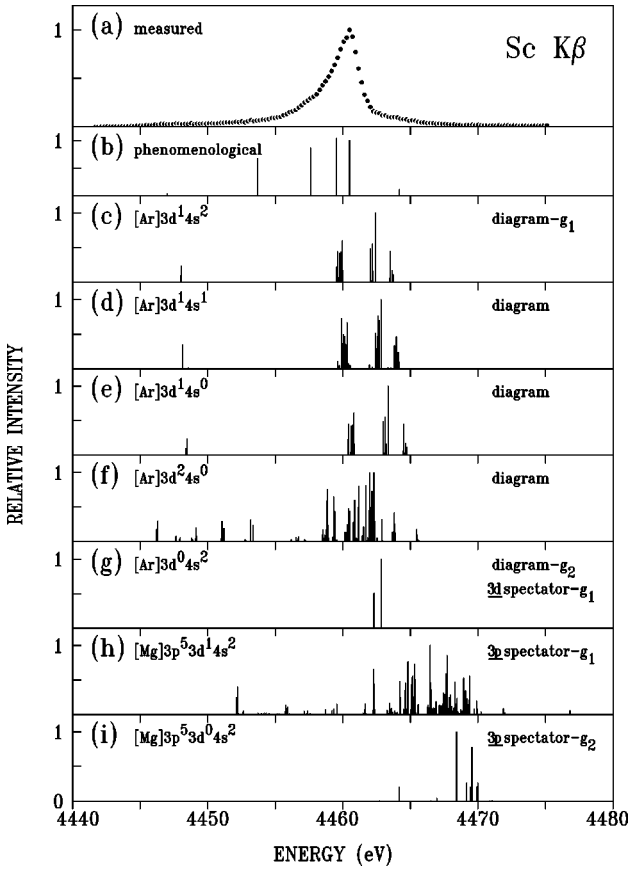

FIG. 9. The $K\beta_{1,3}$ measured spectrum (a), phenomenological fit of Fig. 4(b), and *ab initio* calculated multiplets (c)–(i) for the indicated electronic configurations and transitions. In all frames, the height of individual lines represents the *integrated* intensity of that transition, normalized to the most intense line of the multiplet.

b. Theoretical fits. The diagram transitions giving rise to the $K\alpha_{1,2}$ spectrum, $\underline{1s}\rightarrow\underline{2p}$, involve inner atomic shells

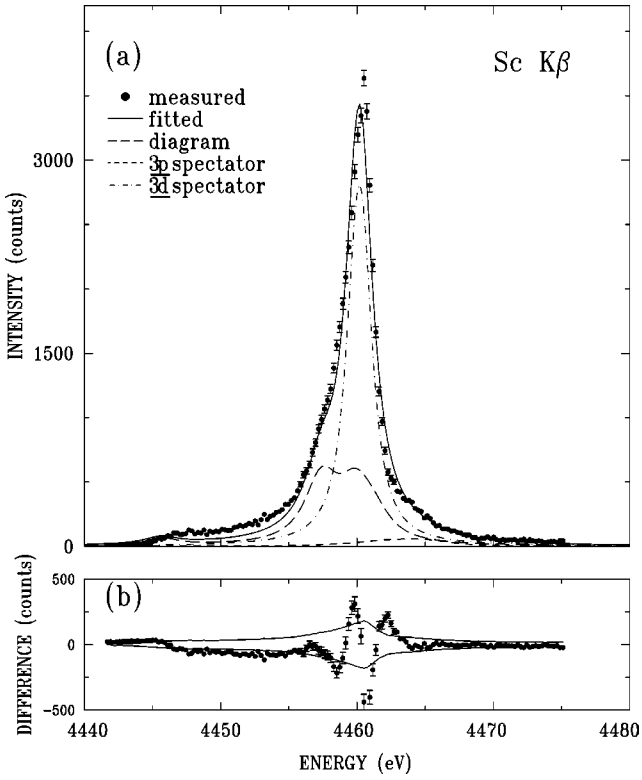

FIG. 10. Fit of the measured $K\beta_{1,3}$ spectrum by the nominal diagram multiplet (c), the $\underline{3p}$-spectator multiplet (h), and the $\underline{3d}$-spectator multiplet (g) in Fig. 9. This fit corresponds to the best fit, fit B, for the $K\alpha_{1,2}$ spectrum, shown in Fig. 7. Note the considerably lower fit quality, indicating the breakdown of the single-atom model.

only. This is not true for the $K\beta_{1,3}$ spectrum, which originates in $\underline{1s}\rightarrow\underline{3p}$ transitions, i.e., involves the $n=3$ valence shell. Thus, the independent-atom approach adopted in our DF calculations and fits, and shown above to account well for the details of the $K\alpha_{1,2}$ spectrum, is not guaranteed to work for the $K\beta_{1,3}$ spectrum. Indeed, even a partial agreement may not be obtainable, as the $3d$ and $3p$ orbitals are expected to be delocalized to some extent and assume a molecular or even a collective, solid-state, nature rather than an isolated atomic one. This conclusion is supported by the detailed study of Kawai *et al.* [10]. Regardless of these results, and wishing to test their validity for metallic Sc, we have attempted to fit the measured $K\beta_{1,3}$ spectrum in a way similar to that of the $K\alpha_{1,2}$ spectrum, namely, using the single-atom model discussed above, with several combinations of the calculated multiplets.

The $K\beta_{1,3}$ fit corresponding to fit B of $K\alpha_{1,2}$ above, i.e., using the nominal $[\mathrm{Ar}]3d^14s^2$ ground state configuration g_1 and including the diagram, the $\underline{3p}$- and the $\underline{3d}$-spectator multiplets are shown in Fig. 10, and the corresponding parameter values are given in Table VIII. Considering the lack of resolved structure in the measured spectrum, we tried to minimize the number of free parameters in the fit to avoid cross correlations. Hence, a fixed resolution width of $w=0.57$ eV, obtained from the exotic atom transition measurements above, was used, and equal widths were assumed for all lines of each multiplet, including the diagram one. As seen in the figure, the fitted spectrum is rather close in shape

TABLE VIII. Fit results for the $K\beta_{1,3}$ scandium spectrum, for the ground-state electronic configuration $[\mathrm{Ar}]3d^14s^2$. Δ, Γ, a_m, and I_{int} denote the shift, width, amplitude, and integrated intensity of each multiplet (see text). $|C+DE|$ (where E is in eV) is the background and w is the full width at half maximum of the Gaussian representing the instrumental resolution function. Reduced χ^2 of the fits are also shown.

Parameters	Transitions	Fit
Δ (eV)	$\underline{1s}\rightarrow\underline{3p}$	−2.38(12)
	$\underline{1s3d}\rightarrow\underline{3p3d}$	−2.50(4)
	$\underline{1s3p}\rightarrow\underline{3p3p}$	−3.30(96)
Γ (eV)	$\underline{1s}\rightarrow\underline{3p}$	2.80(12)
	$\underline{1s3d}\rightarrow\underline{3p3d}$	1.75(8)
	$\underline{1s3p}\rightarrow\underline{3p3p}$	3.08(90)
a_m (counts)	$\underline{1s}\rightarrow\underline{3p}$	2100(96)
	$\underline{1s3d}\rightarrow\underline{3p3d}$	55 430(1500)
	$\underline{1s3p}\rightarrow\underline{3p3p}$	39(10)
C		1.58(2.58)
D		0.0(1)
w (eV)		0.57
I_{int} (%)	$\underline{1s}\rightarrow\underline{3p}$	35
	$\underline{1s3d}\rightarrow\underline{3p3d}$	61
	$\underline{1s3p}\rightarrow\underline{3p3p}$	4
Reduced χ^2		20.85

to the measured one. A more detailed examination, however, and in particular the difference plot in frame (b), reveals serious discrepancies, especially near the peak and along the low-energy tail of the measured line. These deviations result from several features in the calculated multiplets, which we now discuss. Note first the large splitting, mentioned above, and the roughly equal intensities of the two line groups of the calculated diagram spectrum at ~4460 eV and ~4462 eV in Fig. 9(c). This results in a multiplet structure which is significantly broader than the narrow upper part of the measured $K\beta_{1,3}$ line, and thus cannot be fitted to it, regardless of the Lorentzian width parameter adopted for the multiplet. This diagram multiplet is reduced, therefore, in intensity, while the much more narrowly spaced $\underline{3d}$-spectator multiplet [Fig. 9(g)], which is able to reproduce the narrow upper part of the measured lineshape better, gains considerably in intensity. The line and intensity distribution in the two multiplets do not allow, however, a faithful reproduction of the measured $K\beta$ line shape, and a too low peak energy results for the fitted line shape, along with large deviations almost everywhere, as observed in Fig. 10(b). As shown in Table VIII, these deviations are also reflected in the large $\chi^2\approx 21$, threefold that obtained in fit B of $K\alpha_{1,2}$, an anomalous 2.8 eV natural width for the diagram lines, threefold the width calculated theoretically and semiempirically for both the $K\beta_1$ and $K\beta_3$ lines in Table VI, and an inverted diagram/$\underline{3d}$-spectator integrated intensity ratio of 0.57, which should be compared with the $\gtrsim 1$ obtained for $K\alpha_{1,2}$ in Table V. An extensive search was carried out to find a better-fitting combination by allowing different widths for different line

TABLE IX. Radiative Auger K-MM maximal transition energies, in eV, relative to the $K\beta_{1,3}$ peak energy.

KM_iM_j	M_1M_1	$M_1M_{2,3}$	$M_{2,3}M_{2,3}$	$M_1M_{4,5}$	$M_{2,3}M_{4,5}$
$E(KM_iM_j)$-$E(K\beta_{1,3})$	-86.9	-67.4 to -58.0	-42.7 to -38.2	-23.7	-1.5

groups within a multiplet, using the other electronic ground-state configurations given in Fig. 9, and several not listed there, for the diagram and spectator multiplets, etc. None improved the reduced χ^2 values. For example, using the g_2 ground-state in Fig. 9(g) and the corresponding $3p$ spectator in Fig. 9(i) results in the same large $\chi^2 \approx 21$. Other combinations results in even larger χ^2 values.

The measured intensity in the range from 4445 to 4455 eV is observed in Fig. 10 to be consistently higher than the theoretical fit for the g_1 ground-state configuration. By contrast, the $[\mathrm{Ar}]3d^2 4s^0$ configuration, (f) in Fig. 9, shows several lines in this range, not observed for the other ground states, (c)–(e), including g_1. This is in agreement with the study of Pessa *et al.* [36] of Ti ($Z=22$), where the d^2 electrons of the ground-state configuration, $[\mathrm{Ar}]3d^2 4s^2$, yield similar transition lines on the low-energy side of the $K\beta$ spectrum. These were shown there to account qualitatively, if not quantitatively, for the low-energy tail observed for the Ti $K\beta$ line. The existence of such a tail in Sc could be constructed, therefore, as supporting the domination of a similar d^2-electron ground-state configuration in Sc as well. Indeed, Papaconstantopoulos [33] calculates the outer three electrons to be redistributed in the band structure of metallic Sc as 0.71:0.53:1.76 between the *s*-, *p*-, and *d*-like states, respectively, i.e., almost two *d*-like electrons. Nevertheless, attempts to use the corresponding *atomic* configuration (f) as the nominal ground-state in the fits resulted in worse fits than that presented in Fig. 10. It is likely that fits employing band-structure calculations (which are outside the scope of this paper), rather than isolated-atom ones, will be more successful in accounting for the low-energy tail of the measured $K\beta$ spectrum.

We have also looked into the possibility of assigning the deviations in the range from 4445 to 4455 eV to radiative Auger (RA) transitions [37]. In the RA effect the excess energy of the atom following a $\underline{1s} \rightarrow \underline{3p}$ diagram transition is shared between an Auger electron ejected from a higher shell and the emitted x ray photon. This reduces the photon's energy by at least the binding energy E_B of the ejected Auger electron. The maximal photon energy, E_m, for this effect in our case would therefore be $E_m = E_{K\beta} - E_B$. Only the K-MM RA transitions need to be considered in the energy range of this study, and the corresponding shifts of the maximal energy below the $K\beta_{1,3}$ peak, $\Delta E(KM_iM_j)$, can be calculated from [38]

$$\Delta E(KM_iM_j) = E(K\alpha_1) - E(K\beta_{1,3}) + E(L_3M_iM_j), \quad (3)$$

where the three terms on the right-hand side are the energies of the x-ray $K\alpha_1$ and $K\beta_{1,3}$ lines and the Auger $L_3M_iM_j$ line, respectively. Using Bearden's [15] $E(K\alpha_1) = 4090.6$ eV and $E(K\beta_{1,3}) = 4460.5$ eV, and Auger energies from Larkins [39], we obtain the RA maximum energies listed in Table IX. Note that since the $3d$ shell is populated in Sc, RA transitions involving $M_{4,5}$ can occur. Indeed, the table demonstrates that the only RA transition that can possibly contribute in the region under consideration -13.5 to -3 eV below $E(K\beta_{1,3})$ is the $KM_{2,3}M_{4,5}$ one. However, the total intensity expected for the KMM transitions is only $\sim 3\%$ of the $K\beta_{1,3}$ line intensity [38,40], much too low to account for the discrepancies observed. Moreover, the RA intensity goes to a maximum very close to $\Delta E(KM_iM_j)$ and then decays towards lower energies (see, for example, the lower curve in the inset to Fig. 4 of [38]). For the $KM_{2,3}M_{4,5}$ RA transition, which peaks 1.5 eV below the $K\beta_{1,3}$ peak, very little intensity will be left at, say, 5–10 eV below the peak, where the differences between the fitted and the measured spectra in Fig. 10(b) are still considerable. It seems, therefore, that the RA effect cannot account for the discrepancies between the fitted and measured $K\beta_{1,3}$ spectra.

The discussion above leads to the conclusion that although the fit presented in Fig. 10 is the best among the many attempted, it is still insufficient to account for the measured $K\beta_{1,3}$ line shape quantitatively. This implies that the $K\beta_{1,3}$ spectrum cannot be regarded as an isolated-atom spectrum, at least within the single-configuration calculations employed here. The possibility that a multiconfigurational *ab initio* DF calculation, still within the single-atom approximation, may be able to account for the spectral shape cannot be ruled out. However, in view of the conclusion emerging from the detailed study of Kawai *et al.*, that the $3p$ orbital is not fully localized atomically and participates in the collective bonding of the atoms in the solid state, it is much more likely that accounting for the $K\beta_{1,3}$ spectrum requires employing molecular orbitals and/or taking into account band-structure effects.

V. CONCLUSION

The study presented above explored the line shapes of the $K\alpha_{1,2}$ and $K\beta_{1,3}$ spectra of the first $3d$ transition metal. We have measured both scandium spectra with a Johann-type single-crystal spectrometer, the resolution function of which was determined independently using an intrinsically very narrow pionic atom transition. The parameters (widths, asymmetries, etc.) obtained from the measured spectra, using a phenomenological fit by Voigt functions, agree well with previous measurements performed with double-crystal spectrometers. The transitions contributing to the line shape were identified using *ab initio* relativistic Dirac-Fock atomic-structure calculations. Fits of various combinations of the calculated multiplets to the $K\alpha$ spectrum show this spectrum to originate in single-atom transitions and to include contributions from the diagram and the $\underline{3p}$- and $\underline{3d}$-spectator transitions, as found previously for Cu. The contributions from the diagram and the $\underline{3d}$ spectator are found to be roughly equal, while that of the $\underline{3p}$ spectator is about threefold lower. The fit allowed to obtain natural widths for the $K\alpha_{1,2}$ lines,

which are in excellent agreement with theory. Although identified long ago to originate in the $\underline{3p}$-spectator transition, the experimentally observed $K\alpha''$ feature is found here to be just a small part of the total contribution of that transition to the spectrum.

By contrast to the $K\alpha$ results, the line shape of the $K\beta$ spectrum could not be accounted for by multiplets calculated assuming single-atom transitions. It seems probable that this spectrum originates in transitions involving the solid's band structure, as suggested and shown in the study of Kawai *et al.*, based on trends in the chemical-state dependence of the $K\beta$ spectra of scandium compounds. The $K\beta''$ satellite may also originate in such a transition, as suggested by Kawai *et al.*, although its good alignment with the calculated $\underline{3p}$-spectator transition indicates that an alternative assignment to an atomic $\underline{3p}$-spectator transition, similar to that confirmed for the $K\alpha''$ satellite, may also be possible.

Similar studies of the emission spectra of neighboring elements would be required to elucidate the relative importance of molecular bonding and band-structure effects in determining the spectral shape of x-ray emission lines in the early $3d$ transition elements. In particular, near-threshold photoexcitation, now possible at powerful synchrotron sources, allows selective excitation of specific transitions. Such studies should allow a better assessment of the different processes contributing to the spectra and their variation with Z across the $3d$ transition elements.

ACKNOWLEDGMENTS

We gratefully acknowledge important contributions by T. Åberg, J. Utriainen, K. Hämäläinen (Helsinki), J. Kawai (Kyoto), R. Deslattes (Gaithersburg), and P. Indelicato (Paris). We thank the group of Professor J.-P. Egger, University of Neuchâtel, for the use of their CCD detector. M.D. is grateful to the Israel Science Foundation, Jerusalem, for support. D.F.A. thanks the European Union for its support (Marie Curie Institution, Contract No. ERBFMBICT-972448).

[1] J. Kawai, C. Satoko, K. Fujisawa, and Y. Gohshi, Phys. Rev. Lett. **57**, 988 (1986); E.J. Nordgren, Phys. Scr. **T61**, 32 (1996); S. Raj, B.B. Dhal, H.C. Padhi, and M. Polasik, Phys. Rev. B **58**, 9025 (1998); M. Polasik, Phys. Rev. A **58**, 1840 (1998); R. Laihia, J.A. Leiro, K. Kokko, and K. Mansikka, J. Phys.: Condens. Matter **8**, 6791 (1996); I.I. Tupitsyn, L.L. Makarov, and J.F. Batrakov, J. Phys. Chem. Solids **59**, 809 (1998); F.M.F. de Groot, in *Raman Emission by X-Ray Scattering* edited by D.L. Ederer and J.H. McGuire (World Scientific, Singapore, 1996).

[2] M. Deutsch, J. Härtwig, and E. Förster, Phys. Rev. A **56**, 4554 (1997), and references therein.

[3] M. Deutsch, G. Hölzer, J. Härtwig, J. Wolf, M. Fritsch, and E. Förster, Phys. Rev. A **51**, 283 (1995); M. Deutsch, O. Gang, G. Hölzer, J. Härtwig, J. Wolf, M. Fritsch, and E. Förster, *ibid.* **52**, 3661 (1995).

[4] M. Druyvesteyn, Z. Phys. **43**, 707 (1927); Ph.D. thesis, University of Groningen, 1928.

[5] S. Doniach and M. Sunjic, J. Phys. C **3**, 285 (1970).

[6] K. Tsutsumi and H. Nakamori, in *X-Ray Spectra and Electronic Structure of Matter*, edited by A. Faessler and G. Wiech (Fotodruck Frank OHG, München, 1973).

[7] J. Finster, G. Leonhardt, and A. Meisel, J. Phys. (Paris), Colloq. **32**, C-4 (1971).

[8] B.L. Scott, Phys. Rev. A **34**, 4438 (1986).

[9] L.G. Parratt, Phys. Rev. **49**, 502 (1936).

[10] J. Kawai, E. Nakamura, Y. Nihei, K. Fujisawa, and Y. Ghoshi, Spectrochim. Acta B **45**, 463 (1990).

[11] S. Lenz, G. Borchert, H. Gorke, D. Gotta, Th. Siems, D.F. Anagnostopoulos, M. Augsburger, D. Chatellard, J.-P. Egger, D. Belmiloud, P. El-Khoury, P. Indelicato, M. Daum, P. Hauser, K. Kirch, and L.M. Simons, Phys. Lett. B **416**, 50 (1998); Th. Siems *et al.* (unpublished).

[12] D.F. Anagnostopoulos, M. Augsburger, G. Borchert, C. Castelli, D. Chatellard, P. El-Khoury, J.-P. Egger, M. Elble, H. Gorke, D. Gotta, P. Hauser, P. Indelicato, K. Kirch, S. Lenz, N. Nelms, K. Rashid, O.W.B. Schult, Th. Siems, and L.M. Simons, in Proceedings of the Fourth Biennial Conference on Low Energy Antiproton Physics (LEAP 96), edited by H. Koch, M. Kunze, and K. Peters [Nucl. Phys. B (Proc. Suppl.) **56A**, 84 (1997)]; P. Hauser, K. Kirch, L.M. Simons, G. Borchert, D. Gotta, Th. Siems, P. El-Khoury, P. Indelicato, M. Augsburger, D. Chatellard, J.-P. Egger, and D.F. Anagnostopoulos, Phys. Rev. C **58**, 1869 (1998).

[13] D. Gotta *et al.* (unpublished).

[14] M.A. Blokhin, in *Advances in X-ray Spectroscopy*, edited by C. Bonnelle and C. Mandé (Pergamon, Oxford, 1982), pp. 90–103.

[15] J.A. Bearden, Rev. Mod. Phys. **39**, 78 (1967).

[16] G. Fiorucci, D. Bovet, E. Bovet, J.-P. Egger, C. Hêche, C. Nussbaum, D. Schenker, D. Varidel, and J.-M. Vuilleumer, Nucl. Instrum. Methods Phys. Res. A **292**, 141 (1990); D. Varidel, J.-P. Bourquin, D. Bovet, G. Fiorucci, and D. Schenker, *ibid.* **292**, 147 (1990).

[17] S. Boucard and P. Indelicato (private communication).

[18] S. Brennan and P.L. Cowan, Rev. Sci. Instrum. **63**, 850 (1992).

[19] K.G. Dyall, I.P. Grant, C.T. Johnson, F.A. Parpia, and E.P. Plummer, Comput. Phys. Commun. **55**, 425 (1989).

[20] J.W. Cooper, Phys. Rev. A **38**, 3417 (1988); H.P. Saha, *ibid.* **42**, 6507 (1990); M.H. Chen, in *Atomic Inner Shell Physics*, edited by B. Crasemann (Plenum, New York, 1986).

[21] M. Fritsch, C.C. Kao, K. Hämäläinen, O. Gang, and M. Deutsch, Phys. Rev. A **57**, 1686 (1998).

[22] J.A. Bearden and A.F. Burr, Rev. Mod. Phys. **39**, 125 (1967).

[23] The standard deviations (SD's), given in brackets after each value in the tables, were obtained in one of two ways. For values extracted directly from the fit the associated SD's are those evaluated via standard error analysis. When the value cited is a derived quantity X, requiring additional calculations based on the parameters of the fitted curves, a program, written in-house, repeats the required calculation 100 times, varying all relevant parameters randomly within their standard deviations (normally distributed values, with a width equal to the

SD of that particular value). From each calculation the derived quantity X is determined. We then calculate the mean and standard deviation of the 100 values of X. The mean and SD are then listed in the table as the value and its error. For example, the FWHM $= 1.332 \pm 0.016$ eV listed for $K\alpha_1$ in the line denoted ''Run I'' in Table II was calculated by computing 100 times the sum of the six VF's, using the parameters listed in Table I. In each calculation the value of each parameter was chosen randomly within the range permitted by the SD of that parameter, as listed in brackets in Table I. For each sum, the FWHM of $K\alpha_1$ was determined. The mean of the 100 values was calculated to be 1.332, and the SD from the mean was 0.016.

[24] V.M. Pessa, X-Ray Spectrom. **2**, 169 (1973).
[25] S.K. Allison, Phys. Rev. **44**, 63 (1933).
[26] J.A. Bearden and C.H. Shaw, Phys. Rev. **48**, 18 (1935).
[27] P. Sarode, X-Ray Spectrom. **22**, 138 (1993).
[28] D.A. Shirley, R.L. Martin, S.P. Kowalczyk, F.R. McFeely, and L. Ley, Phys. Rev. B **15**, 544 (1977).
[29] M. Cardona and L. Ley, *Photoemission from Solids* (Springer, Berlin, 1978).
[30] S.I. Salem and R.J. Wimmer, Phys. Rev. A **2**, 1121 (1970).
[31] U.D. Misra, M. Sah, and B.G. Gokhale, J. Phys. B **25**, 4107 (1992).
[32] Photoelectron spectroscopy measurements for the elemental solids, as cited in Table I of K.D. Sevier, At. Data Nucl. Data Tables **24**, 323 (1979).
[33] D.A. Papaconstantopoulos, *Handbook of the Band Structure of Elemental Solids* (Plenum, NY, 1986), pp. 75–77; N. Papanicolaou (private communication).
[34] P.H. Citrin, P.M. Eisenberger, W.C. Marra, T. Åberg, J. Utriainen, and E. Källne, Phys. Rev. B **B10**, 1762 (1974); E. Källne, in *Encyclopedia of Physics*, edited by R.G. Lerner and G.L. Trigg (Addison-Wesley, London, 1952), p. 1113.
[35] B. Crasemann and M.H. Chen (private communication).
[36] M. Pessa, E.-K. Kortela, A. Suikkanen, and E. Suoninen, Phys. Rev. A **8**, 48 (1973).
[37] T. Åberg and J. Utriainen, Phys. Rev. Lett. **22**, 1346 (1969); H. Hayashi, N. Watanabe, and Y. Udagawa, J. Phys.: Condens. Matter **8**, 37 (1996).
[38] A. Mühleisen, M. Budnar, and J.-Cl. Dousse, Phys. Rev. A **54**, 3852 (1996).
[39] P. Larkins, At. Data Nucl. Data Tables **20**, 311 (1977).
[40] J. Utriainen, M. Linkoaho, and T. Åberg (unpublished).
[41] E.J. McGuire, Phys. Rev. A **2**, 273 (1970).
[42] E.J. McGuire, Phys. Rev. A **3**, 587 (1971).
[43] E.J. McGuire, Phys. Rev. A **5**, 1043 (1972).
[44] M.H. Chen, B. Crasemann, and H. Mark, Phys. Rev. A **21**, 436 (1980).
[45] M.H. Chen, B. Crasemann, and H. Mark, Phys. Rev. A **24**, 177 (1981).
[46] L.I. Yin, I. Adler, T. Tsang, M.H. Chen, D.A. Ringers, and B. Crasemann, Phys. Rev. A **9**, 1070 (1974).
[47] M.O. Krause and J.H. Oliver, J. Phys. Chem. Ref. Data **8**, 329 (1979).
[48] S.T. Perkins, D.E. Cullen, M.H. Chen, J.H. Hubbell, J. Rathkopf, and J. Scofield, Lawrence Livermore National Laboratory, Evaluated Atomic Data Library (EADL) $Z = 1 - 100$, Report No. UCRL-50400, 1991.
[49] W.J. Kuhn and B.L. Scott, Phys. Rev. A **34**, 1125 (1986).